Correlation-based decomposition of surface electromyograms at low contraction forces

A. Holobar **D. Zazula**

Faculty of Electrical Engineering & Computer Science, University of Maribor, Maribor, Slovenia

Abstract—*The paper studies a surface electromyogram (SEMG) decomposition technique suitable for identification of complete motor unit (MU) firing patterns and their motor unit action potentials (MUAPs) during low-level isometric voluntary muscle contractions. The algorithm was based on a correlation matrix of measurements, assumed unsynchronised (uncorrelated) MU firings, exhibited a very low computational complexity and resolved the superimposition of MUAPs. A separation index was defined that identified the time instants of an MU's activation and was eventually used for reconstruction of a complete MU innervation pulse train. In contrast with other decomposition techniques, the proposed approach worked well also when the number of active MUs was slightly underestimated, if the MU firing patterns partly overlapped and if the measurements were noisy. The results on synthetic SEMG show 100% accuracy in the detection of innervation pulses down to a signal-to-noise ratio (SNR) of 10 dB, and 93 ± 4.6% (mean ± standard deviation) accuracy with 0 dB additive noise. In the case of real SEMG, recorded with an array of 61 electrodes from biceps brachii of five subjects at 10% maximum voluntary contraction, seven active MUs with a mean firing rate of 14.1 Hz were identified on average.*

Keywords—*Surface electromyography, Compound signal decomposition, Reconstruction of motor-unit firing patterns, Extraction of motor-unit action potentials, Correlation-based decomposition*

Med. Biol. Eng. Comput., 2004, **42**, 487–495

1 Introduction

DECOMPOSITION OF EMG signals to motor unit (MU) firing patterns has proved to be a very important clinical issue. Reconstructed sequences of innervation pulses provide the basis for research studies and clinical examinations of MU control properties (DE LUCA *et al.*, 1996), recruitment strategies (FALLENTIN *et al.*, 1993), inter-pulse interval (IPI) variability (CLANCY and HOGAN, 1999), short-term MU synchronisation (WEYTJENS and VAN STEENBERHE, 1984) and myo-electrical manifestations of fatigue (MERLETTI *et al.*, 1994), to name just a few areas of investigation.

Existing computer-aided EMG decomposition methods have been mainly focused on the intra-muscular EMG signals. Being based on pattern recognition and clustering in the time domain, on spatial filters and on time-scale analysis, they typically exploit the differences in morphology of motor unit action potentials (MUAPs) and comprise two steps (FARINA *et al.*, 2001). First, an individual MUAP is identified from the raw inter-muscular EMG. Afterwards, the identified MUAP is classified and assigned to the best-fit class of previous by decomposed MUAP shapes. Unfortunately, most of the methods fail when MUAPs become superimposed. As a result, the complete decomposition is possible only if the number of simultaneously active MUs is relatively small.

In the case of surface EMG (SEMG) signals, the filtering effect of subcutaneous tissue, which separates the detection system from the MUs, attenuates the morphological differences of MUAPs (MERLETTI, 1994). Nevertheless, the non-invasive nature of SEMG and its wide potential to offer global information about muscle activity have opened numerous application areas. The information extracted from SEMG signals is being exploited in several different clinical studies, mainly concerned with the timing of the muscle activation (MICERA *et al.*, 2001), the EMG amplitude modulation (CLANCY and HOGAN, 1999), changes in the frequency content of the EMG signals (BALESTRA *et al.*, 2001) and conduction velocity estimation (FARINA *et al.*, 2000).

However, the decomposition of SEMG signals to constituent MUAP trains, even at low muscle contractions, still remains a very delicate process. The main difficulty is the high SEMG signal complexity. In addition to a high number of superimposed MUAPs, no *a priori* information about the nature of their mixture is available; hence, SEMG signals should be decomposed blindly (AMARI *et al.*, 2002). Only recently, some more

Correspondence should be addressed to Dr Ales Holobar; email: ales.holobar@uni-mb.si

Paper received 31 October 2003 and in final form 29 April 2004

MBEC online number: 20043916

sophisticated decomposition methods have begun to emerge. Exploiting advanced signal processing techniques, they provide new insights of clinical interest as they, for example, work towards removal of artifacts (BARROS *et al.*, 1999) and the identification of the EMG constituent MUAPs (HOLOBAR and ZAZULA, 2003).

Most recent advances in SEMG decomposition show very promising applications of time-frequency (TF) analysis (HOLOBAR and ZAZULA, 2003) and higher-order statistics (HOSs) (ZAZULA and PLEVIN, 2002). The former has been proven to work with short, few seconds long, artificial surface EMG, perfectly deconvolving it to the innervation trains. On the other hand, HOS-based techniques were shown to extract correctly the shapes of MUAPs, even when the measurements were highly contaminated with noise (ZAZULA and PLEVIN, 2002).

In this paper, a novel blind decomposition based on the inverse correlation of multichannel surface EMG signals is introduced. The technique follows the approaches in HOLOBAR and ZAZULA (2003) and ZAZULA and PLEVIN (2002) by modelling the MUAPs as a unit sample response of a multiple-input-multiple-output (MIMO) linear, time-invariant (LTI) system. As such, it assumes stationary MUAPs with unchangeable shape and unsynchronised MUs and is, hence, appropriate for the decomposition of SEMG recorded during isometric muscle contraction at low contraction force. Contrary to the TF approach (HOLOBAR and ZAZULA, 2003), it enables the reconstruction of entire innervation pulse trains of arbitrary length, even when the number of superimposed MUAPs is high.

Although the derivation presumes more measurements than sources, i.e. active MUs, it can be applied when the number of active MUs is slightly higher than SEMG measurements (throughout the paper we will understand the measurements as SEMG recordings). The preliminary tests on synthetic and real surface EMG signals of biceps brachii muscle prove the method to be a useful tool in both research and clinical investigations.

2 Correlation-based decomposition

2.1 *Data model*

With the assumption of isometric muscle contractions at constant contraction forces, the multichannel surface EMG can be modelled as an LTI MIMO system (ZAZULA and PLEVIN, 2002). Each channel in such a system is considered an MU, with its response in the form of an MUAP as captured by a surface electrode, and the channel inputs correspond to the innervation pulse trains

$$x_i(n) = \sum_{j=1}^{N} \sum_{l=0}^{L-1} h_{ij}(l) s_j(n-l) + w_i(n) \quad i = 1, \ldots, M \tag{1}$$

where, taking multiple inputs and outputs, the vector notations are as follows: $\boldsymbol{x}(n) = [x_1(n), \ldots, x_M(n)]^T$ for the transposed vector of M discrete (sampled) surface EMG measurements; $\boldsymbol{s}(n) = [s_1(n), \ldots, s_N(n)]^T$ for the vector of N trains of pulses (sources); and $\boldsymbol{w}(n) = [w_1(n), \ldots, w_M(n)]^T$ for the noise vector. $h_{ij}(l)$; $l = 0, \ldots, L-1$, stands for the MUAP (unit sample response with length L) of the jth source as detected by the ith electrode. We further suppose the number of measurements to be greater than the number of sources, $M > N$.

The additive noise $w_i(n)$ is commonly modelled as a stationary, temporally and spatially white, zero-mean Gaussian random process, being independent from the sources

$$E[\boldsymbol{w}(n+\tau)\boldsymbol{w}^*(n)] = \sigma^2 \delta(\tau) \boldsymbol{I} \tag{2}$$

where $E[\cdot]$ stands for mathematical expectation, $\delta(\cdot)$ stands for the Dirac impulse (delta function), σ^2 stands for the noise variance, and $\boldsymbol{I}$ denotes the identity matrix.

Our goal in blind SEMG decomposition is to reconstruct the source pulse trains $\boldsymbol{s}(n) = [s_1(n), \ldots, s_N(n)]^T$, given only the vector of measurements $\boldsymbol{x}(n) = [x_1(n), \ldots, x_M(n)]^T$. To extend (1) to a convolutive MIMO vector form, the vector $\boldsymbol{x}(n)$ has to be augmented by K delayed repetitions of each measurement

$$\bar{\boldsymbol{x}}(n) = [x_1(n), x_1(n-1), \ldots, x_1(n-K+1), \ldots, x_M(n), \ldots, x_M(n-K+1)]^T \tag{3}$$

where K is an arbitrary large integer that satisfies

$$KM > N(L+K) \tag{4}$$

Extending the noise vector in the same manner, (1) can be rewritten in a vector form

$$\bar{\boldsymbol{x}}(n) = \boldsymbol{H}\bar{\boldsymbol{s}}(n) + \bar{\boldsymbol{w}}(n) \tag{5}$$

$\boldsymbol{H}$ in (5) stands for the so-called mixing matrix of size $KM \times N(L+K)$ that contains the unit sample responses $h_{ij}(l)$

$$\boldsymbol{H} = \begin{bmatrix} \boldsymbol{H}_{11} & \cdots & \boldsymbol{H}_{1N} \\ \vdots & \ddots & \vdots \\ \boldsymbol{H}_{M1} & \cdots & \boldsymbol{H}_{MN} \end{bmatrix} \tag{6}$$

with

$$\boldsymbol{H}_{ij} = \begin{bmatrix} h_{ij}(0) & \cdots & h_{ij}(L) & \cdots & 0 \\ \vdots & \ddots & \ddots & \ddots & \vdots \\ 0 & \cdots & h_{ij}(0) & \cdots & h_{ij}(L) \end{bmatrix} \tag{7}$$

and the extended vector of sources $\boldsymbol{s}(n)$ takes the following form:

$$\bar{\boldsymbol{s}}(n) = [s_1(n), \ldots, s_1(n-L-K+1), \ldots, s_N(n), \ldots, s_N(n-L-K+1)]^T \tag{8}$$

Following the above assumptions, the correlation matrix of extended measurements can be expressed as

$$\boldsymbol{R}_{\bar{x}} = \lim_{T \to \infty} \frac{1}{T} \sum_{n=1}^{T} \bar{\boldsymbol{x}}(n)\bar{\boldsymbol{x}}^*(n) = \boldsymbol{H}\boldsymbol{R}_{\bar{s}}\boldsymbol{H}^T + \sigma^2 \boldsymbol{I} \tag{9}$$

where $\boldsymbol{R}_{\bar{s}}$ denotes the correlation matrix of sources, and $\bar{\boldsymbol{x}}^*(n)$ stands for the conjugate transpose of $\bar{\boldsymbol{x}}(n)$.

2.2 *Blind decomposition using the inverse correlation matrix*

According to (4), there are at least $KM - N(L+K)$ eigenvalues of $\boldsymbol{R}_{\bar{x}}$ equal to σ^2. Consequently, the noise variance $\hat{\sigma}^2$ can be estimated by averaging of the $KM - N(L+K)$ smallest eigenvalues of $\boldsymbol{R}_{\bar{x}}$. Subtracting it from the correlation matrix of measurements, we obtain

$$\bar{\boldsymbol{R}}_{\bar{x}} = \boldsymbol{R}_{\bar{x}} - \hat{\sigma}^2 \boldsymbol{I} = \boldsymbol{H}\boldsymbol{R}_{\bar{s}}\boldsymbol{H}^T \tag{10}$$

Supposing the mixing matrix $\boldsymbol{H}$ of a full column rank $rank(\boldsymbol{H}) = N(L+K)$, we introduce the so-called MU activity index

$$\begin{aligned} Ind(n) &= \bar{\boldsymbol{x}}(n)^T \bar{\boldsymbol{R}}_{\bar{x}}^{-1} \bar{\boldsymbol{x}}(n) \\ &= \bar{\boldsymbol{s}}(n)^T \boldsymbol{H}^T (\boldsymbol{H}\boldsymbol{R}_{\bar{s}}\boldsymbol{H}^T)^{-1} \boldsymbol{H}\boldsymbol{s}(n) + v_{\bar{w}}(n) \\ &= \bar{\boldsymbol{s}}(n)^T \boldsymbol{H}^T (\boldsymbol{H}^T)^{-1} \boldsymbol{R}_{\bar{s}}^{-1} \boldsymbol{H}^{-1} \boldsymbol{H}\boldsymbol{s}(n) + v_{\bar{w}}(n) \\ &= \bar{\boldsymbol{s}}(n)^T \boldsymbol{R}_{\bar{s}}^{-1} \bar{\boldsymbol{s}}(n) + v_{\bar{w}}(n) \end{aligned} \tag{11}$$

where superscript $^{-1}$ denotes the matrix inverse, and $v_{\bar{w}}(n)$ replaces the impact of all noise. If we neglect the influence of noise, the activity index $Ind(n)$ could be thought of as an

indicator of a global source activity. It differs from zero only at the time instant where at least one source is active. Moreover, its value increases with the number of simultaneously active sources. The reverse is not generally true. A high value of the activity index can either be the consequence of a bigger number of active sources or can indicate the activity of only one source with a low firing rate (a higher 'weight' on the diagonal of $\boldsymbol{R}_{\bar{s}}^{-1}$).

2.2.1 *Noise-free decomposition:* When a sample index n_0 is found in which only the jth source is active the entire pulse train of the jth source can be reconstructed as

$$p_{n_0,j}(n) = \bar{\boldsymbol{x}}(n_0)^T \bar{\boldsymbol{R}}_{\bar{x}}^{-1} \bar{\boldsymbol{x}}(n) = \bar{\boldsymbol{s}}(n_0)^T \boldsymbol{R}_{\bar{s}}^{-1} \bar{\boldsymbol{s}}(n) = r_{j,j} \bar{s}_j(n_0) \bar{s}_j(n) \quad (12)$$

where $r_{j,j}$ denotes the (j,j)th element of $\boldsymbol{R}_{\bar{s}}^{-1}$. If Q_{n_0} sources, denoted by the group of indices $G_{n_0} = \{j_{n_0,1}, \ldots, j_{n_0,Q_{n_0}}\}$, are active at given sample index n_0, (12) yields the superimposition of innervation pulses of all these sources at n_0:

$$\begin{aligned} p_{n_0,G_{n_0}}(n) = {} & r_{j_{n_0,1},j_{n_0,1}} \bar{s}_{j_{n_0,1}}(n_0) \bar{s}_{j_{n_0,1}}(n) \\ & + r_{j_{n_0,1},j_{n_0,2}} \bar{s}_{j_{n_0,1}}(n_0) \bar{s}_{j_{n_0,2}}(n) \\ & + \cdots + r_{j_{n_0,1},j_{n_0,Q_{n_0}}} \bar{s}_{j_{n_0,1}}(n_0) \bar{s}_{j_{n_0,2}}(n) \\ & + r_{j_{n_0,2},j_{n_0,1}} \bar{s}_{j_{n_0,2}}(n_0) \bar{s}_{j_{n_0,1}}(n) \\ & + r_{j_{n_0,2},j_{n_0,2}} \bar{s}_{j_{n_0,2}}(n_0) \bar{s}_{j_{n_0,2}}(n) \\ & + \cdots + r_{j_{n_0,Q_{n_0}},j_{n_0,Q_{n_0}}} \bar{s}_{j_{n_0,Q_{n_0}}}(n_0) \bar{s}_{j_{n_0,Q_{n_0}}}(n) \end{aligned} \quad (13)$$

Although (12) resolves our decomposition problem entirely, the situation from (13) needs further processing. We must separate the overlapping sources having only the information from (13). The randomness of innervation pulse trains contributes crucially to the proposed solution. With low contraction forces, the innervation pulse trains do not overlap significantly (up to a few percent). Consequently, matrix $\boldsymbol{R}_{\bar{s}}$ tends to have high diagonal elements in comparison with off-diagonal ones. The same then holds for its inverse $\boldsymbol{R}_{\bar{s}}^{-1}$ (GOLUB and VAN LOAN, 1989), and the contributions of the auto-terms $r_{j,j} \bar{s}_j(n_0) \bar{s}_j(n)$ in (13) can be expected to be much higher than the cross-term contributions $r_{j_1,j_2} \bar{s}_{j_1}(n_0) \bar{s}_{j_2}(n)$, $j_1 \neq j_2$.

Looking for the highest values inside $p_{n_0,G_{n_0}}(n)$, the probability to find a sample index n_1 corresponding to the firing moment of another group of sources G_{n_1} is rather high. Applying the calculation from (12) in n_1, a superimposition of active sources G_{n_1} appears analogously to (13): $p_{n_1,G_{n_1}}(n)$. Again, because of the nature of the innervation pulse trains it is highly unlikely that $G_{n_0} = G_{n_1}$, which means that a selection of simultaneous pulses in $p_{n_0,G_{n_0}}(n)$ and $p_{n_1,G_{n_1}}(n)$ sorts out only those fewer sources that fire at both n_0 and n_1. The proposed elimination can be repeated until the superimposed sources detected at sample index n_0 are completely separated.

2.2.2 *Noisy case:* In practice, the activity index and any reconstructed pulse sequences are additionally corrupted by the noise component

$$v_{\bar{w}}(n) = 2\bar{\boldsymbol{w}}(n)^T (\boldsymbol{H}^T)^{-1} \boldsymbol{R}_{\bar{s}}^{-1} \bar{\boldsymbol{s}}(n) + \bar{\boldsymbol{w}}(n)^T (\boldsymbol{H}^T)^{-1} \times \boldsymbol{R}_{\bar{s}}^{-1} \boldsymbol{H}^{-1} \bar{\boldsymbol{w}}(n) \quad (14)$$

If the noises $\bar{w}_i(n)$ are assumed to be white, zero-mean Gaussian, they would reflect in the space of sources as coloured, zero-mean Gaussian. Analysing the right-hand side of (14), it is obvious that the first term does not hinder the decomposition process, because it can merely alter the power (height) of the triggering pulses. However, the second term might appear much more devastating. It corrupts $p_{n_k,G_{n_k}}(n)$ at every possible sample index n, which can make the source-separation approach described for the noise-free case practically unfeasible. The necessary noise reduction can be implemented either in the space of measurements or in the space of sources. Assuming the measurement-additive noises to be uncorrelated in time and in space, noise reduction through averaging is most obvious. Various noise reduction techniques were tested in this study. The best results were obtained by averaging several estimates of each innervation train, as detailed in the algorithm outlined below.

2.3 *Decomposition algorithm*

The proposed decomposition procedure can be summarised in the following eight steps:

Step 1: Take a multichannel surface SEMG recording of isometric muscle contraction and extend the measurements according to (3). The number of repetitions K is given by (4).

Step 2: Calculate the correlation matrix of extended measurements, estimate noise variance and apply (10) and (11) to calculate the activity index.

Step 3: Select initial index n_0 for which $Ind(n_0)$ exceeds a predefined noise threshold, $\hat{\sigma}^2 \sum_{i=1}^{KM} \bar{r}_{i,i}$, where $\bar{r}_{i,i}$ denotes the (i,i)th element of $\bar{\boldsymbol{R}}_{\bar{x}}^{-1}$, and filter out the pulse sequence according to (12).

Step 4: In a reconstructed train of pulses, find the highest pulse according to (13), denote its position by n_1 and calculate $p_{n_1,G_{n_1}}(n)$ as in (12).

Step 5: Find sample indices n_j; $j = 2, 3, \ldots, Q$ (Q is an arbitrary integer satisfying $Q > K$) belonging to the Q highest peaks in the product $p_{n_0,G_{n_0}}(n) \cdot p_{n_1,G_{n_1}}(n)$. If the calculation from (12) is applied in all n_j sample indices, Q additional sequences $p_{n_j,G_{n_j}}(n)$ are obtained.

Step 6: Only those sequences having positive value at n_0, $p_{n_j,G_{n_j}}(n_0) > 0$, are averaged to yield the final innervation train estimation of one single source.

Step 7: Compare the obtained innervation train with all previously reconstructed pulse sequences. Thus the obtained train is classified as either a new one or as already detected.

Step 8: Repeat steps 3–7 until any sample index n_k exists where the global activity index $Ind(n_k)$ exceeds the noise threshold defined in step 3.

For each reconstructed innervation pulse train, the corresponding MUAPs can be obtained by a spike-triggered sliding-window averaging technique (DISSELHORST-KLUG *et al.*, 1999).

3 Simulations and experiments

3.1 *Synthetic signals*

To verify the proposed method, synthetic surface EMG signals were generated using the advanced EMG simulator (FARINA and MERLETTI, 2001). The influence of two factors was evaluated during our simulation: the number of active MUs and the signal-to-noise ratio (SNR). The number of active MUs was set to 5, 10 and 20, respectively, and the SNR ranged from 0 dB to 20 dB, in steps of 5 dB. The other important SEMG parameters were set as follows:

(*a*) Skin was simulated as a 1 mm thick isotropic layer, and subcutaneous fatty tissue was simulated as a 3 mm thick isotropic layer.

(*b*) Active MUs consisted of a random number of fibres (uniformly distributed between 50 and 300) with the circular MU territories of 20 fibres mm^{-2}. The depth of

Table 1 Number of reconstructed MU firing patterns (mean ± SD) and average firing rate (mean ± SD), average MU depth in muscle tissue (mean ± SD) and average number of fibres (mean ± SD) of identified (+) and missed (−) MUs against number of active MUs and SNR. Normalised values of morphological index (15) are depicted (mean ± SD) in right-most column. Results were obtained on synthetic SEMG signals

Number of simulated MUs	SNR, dB	Average number of detected MUs	Average firing rate		Average depth in muscle tissue		Average number of fibres		Average morphological index $I_{f,A}$	
			+	−	+	−	+	−	+	−
5	20	4.7 ± 0.6	15.5 ± 3.5	15.3 ± 3.9	6.1 ± 1.0	8.3 ± 0.6	156 ± 53	129 ± 65	0.55 ± 0.24	0.23 ± 0.14
	15	4.2 ± 0.6	15.3 ± 3.0	15.9 ± 3.1	6.1 ± 1.0	7.9 ± 1.5	168 ± 45	98 ± 41	0.61 ± 0.21	0.25 ± 0.18
	10	3.9 ± 0.7	15.6 ± 3.2	15.4 ± 3.4	6.1 ± 1.0	7.1 ± 1.4	175 ± 40	96 ± 34	0.63 ± 0.20	0.28 ± 0.19
	5	3.2 ± 0.6	15.5 ± 3.2	15.7 ± 3.4	5.9 ± 0.8	6.8 ± 1.4	173 ± 41	116 ± 53	0.65 ± 0.21	0.32 ± 0.12
	0	2.0 ± 0.9	15.3 ± 3.3	15.5 ± 3.6	5.8 ± 0.4	6.8 ± 1.4	188 ± 40	124 ± 43	0.70 ± 0.22	0.39 ± 0.15
10	20	8.3 ± 1.3	16.0 ± 2.8	14.9 ± 3.8	6.6 ± 1.0	7.8 ± 1.0	161 ± 47	93 ± 50	0.57 ± 0.22	0.29 ± 0.18
	15	7.0 ± 1.6	15.9 ± 2.9	14.9 ± 2.9	6.6 ± 1.0	6.8 ± 0.9	165 ± 45	100 ± 51	0.59 ± 0.22	0.30 ± 0.19
	10	6.4 ± 1.9	16.0 ± 2.7	15.2 ± 2.8	6.4 ± 1.0	6.5 ± 0.8	170 ± 46	109 ± 46	0.63 ± 0.19	0.31 ± 0.17
	5	4.6 ± 1.7	15.9 ± 2.8	15.0 ± 2.8	6.0 ± 0.9	6.5 ± 0.9	178 ± 48	124 ± 47	0.67 ± 0.16	0.39 ± 0.22
	0	2.6 ± 1.4	15.9 ± 2.8	15.8 ± 2.9	6.1 ± 0.8	6.4 ± 1.0	200 ± 36	132 ± 49	0.68 ± 0.17	0.46 ± 0.24
20	20	10.4 ± 1.4	15.1 ± 3.2	15.7 ± 2.5	6.0 ± 0.6	7.2 ± 0.9	171 ± 40	125 ± 52	0.49 ± 0.18	0.26 ± 0.14
	15	8.6 ± 1.7	15.8 ± 2.7	15.0 ± 3.6	6.0 ± 0.7	7.0 ± 1.0	176 ± 40	128 ± 50	0.53 ± 0.17	0.27 ± 0.13
	10	5.7 ± 1.3	15.0 ± 3.2	15.9 ± 2.9	5.9 ± 0.5	6.9 ± 1.0	176 ± 48	138 ± 49	0.55 ± 0.18	0.31 ± 0.16
	5	3.5 ± 1.3	15.9 ± 3.0	16.0 ± 2.7	5.7 ± 0.5	6.8 ± 1.0	203 ± 25	139 ± 49	0.69 ± 0.13	0.33 ± 0.15
	0	2.3 ± 1.9	16.0 ± 2.8	15.9 ± 2.7	5.7 ± 0.3	6.5 ± 1.0	206 ± 24	142 ± 50	0.70 ± 0.14	0.34 ± 0.17

active MUs in the anisotropic muscle layer varied uniformly from 3 mm to 10 mm, and additional random shift (uniformly distributed between −10 and 10 mm) from the centre of the electrode array in the direction transverse to the muscle fibres was applied to each MU.

(*c*) The MU firing rate was normally distributed around the mean of 15 Hz, with standard deviation of 4 Hz. The IPI variability was modelled as a zero-mean Gaussian variable with the variance equal to 20% of the IPI mean.

(*d*) Conduction velocity was assumed to be normally distributed, with a mean of 4 m s^{-1} and standard deviation of 1 m s^{-1}.

(*e*) The innervation zones were assumed to be placed in the middle between the tendons, and the semi-fibre length was set to 70 mm. The spread of innervation zones was limited to 5 mm.

(*f*) A 10 × 5 array detection system with ten rows and five electrodes per row was centred over the innervation zone, the columns aligned with the direction of the fibres.

(*g*) Rectangular 1 × 1 mm electrodes with an inter-electrode distance of 5 mm were simulated. Measurements were assumed to be single-differential.

(*h*) Synthetic SEMG signals of 30 s duration, were sampled at 1024 Hz.

Twenty simulations were performed for each number of active MUs. In each of the simulation runs, the depth of the active MUs, their firing rate, number of fibres, shift in the direction transverse to the muscle fibres and conduction velocity were randomly selected. In addition, signals from each simulation run were corrupted by additive noise (eight realisations of noise for each SNR), resulting in 800 test signals for each number of active MUs.

3.2 *Experimental protocol with real SEMG*

The experiments were conducted with signals from the dominant biceps brachii, recorded in Laboratorio di Ingegneria del Sistema Neuromuscolare (LISiN), Politecnico di Torino, Italy. Five healthy male subjects of age 27.8 ± 2.4 years, height 177.2 ± 4.5 cm and weight 70.6 ± 4.9 kg participated in our study. Surface EMG signals were detected by an array of 13 × 5 electrodes (without the four corner electrodes) of size 1 × 1 mm and of inter-electrode distance 5 mm. The experimental protocol was as follows:

(i) The dominant arm of the subject was placed into the isometric brace at 120°. The skin was slightly abraded with abrasive paste and moistened to improve the electrode–skin contact.

(ii) Three 5s contractions at maximum voluntary contraction (MVC) force were performed, separated by 2 min. Afterwards, a 5 min rest was allowed to the subject.

(iii) The location of the innervation zone in the dominant biceps brachii of the subject was determined using a linear array of 16 electrodes of size 10 × 1 mm and inter-electrode distance of 10 mm.

(iv) The array of 61 electrodes was placed over the biceps, with its third electrode row centred over the innervation zone and columns aligned with the muscle fibres.

(v) SEMGs of 30 s were recorded at isometric voluntary contractions sustained at 5% and 10% of MVC. After each contraction, the subject relaxed for 5 min.

The detected signals were amplified (gain set to 10^4) by a 64-channel EMG amplifier*, bandpass filtered (−3 dB bandwidth, 10–500 Hz) and sampled at 2048 Hz by a 12-bit analogue-to-digital (AD) converter. A longitudinal single-differential recording technique was used with the adjacent electrode pairs along the columns in the electrode array, resulting in 56 SEMG recordings. The noise and movement artifacts were visually controlled and reduced by the application of water to the skin surface. The contraction force was measured by the torque sensor and displayed on the oscilloscope to provide the visual feedback to the subjects. Before any further processing, all the measurements were digitally filtered to suppress the 50 Hz interference. However, to preserve their original shape, the MUAPs were averaged from unfiltered measurements.

*LISiN; Prima Biomedical & Sport, Treviso, Italy

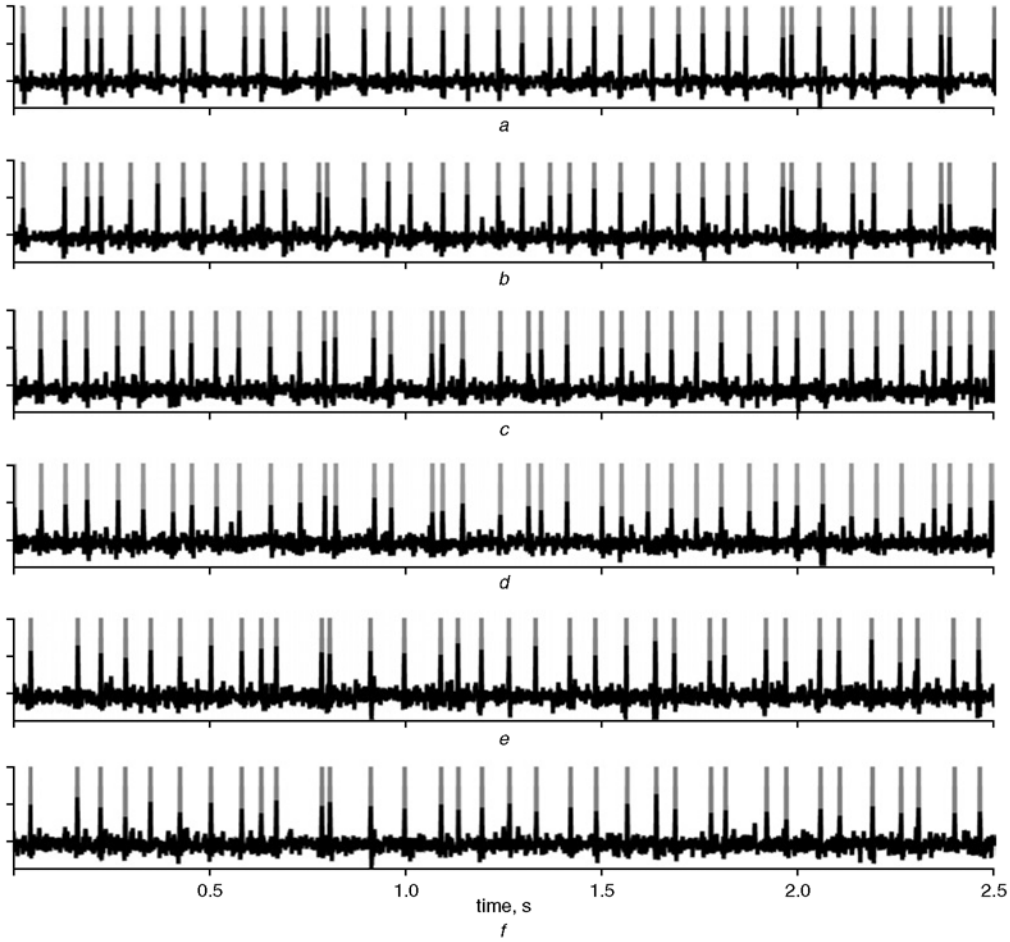

Fig. 1 *(■) Original synthetic MU innervation train and (■) reconstructed innervation train. Owing to simulation protocol (MU parameters were randomly generated for each number of active MUs), results for different, but morphologically similar, MUs are depicted: MU (177 fibres, depth: 5.3 mm, firing rate: 15.2 Hz) in case of 5 active MUs, reconstructed at (a) SNR = 10 dB and (b) SNR = 5 dB; MU (181 fibres, depth: 5.2 mm firing rate: 15.7 Hz) reconstructed in case of 10 active MUs at (c) SNR = 10 dB and (d) SNR = 5 dB; MU (191 fibres, depth: 5.2 mm, firing rate: 14.7 Hz) reconstructed in case of 20 active MUs at (e) SNR = 10 dB and (f) SNR = 5 dB*

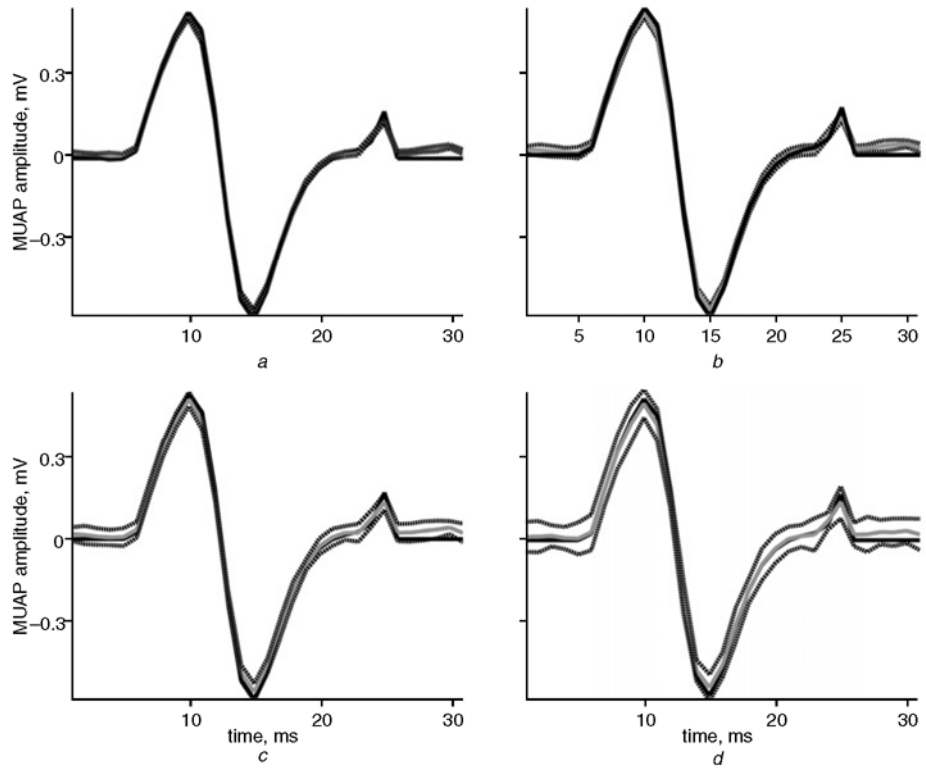

Fig. 2 *Action potentials ((——) mean value; (– – –) standard deviation) of MU (191 fibres, depth: 5.2 mm, firing rate: 14.7 Hz) reconstructed by spike-triggered sliding window averaging technique in case of 20 active MUs and (– · – ·) their reference values: (a) SNR = 20 dB; (b) SNR = 15 dB; (c) SNR = 10 dB; (d) SNR = 5 dB*

4 Decomposition results

4.1 *Decomposition of synthetic signals*

The influence of the MU firing rate, the depth of MUs in the muscle tissue and the number of MU fibres were investigated on synthetic SEMGs. The theory predicts a decomposition performance drop with increasing MU firing rate. MUs with high firing rates are expected to have high zero-lag correlation, which attenuates the detected firing pulses in (12). The performance should also drop if the MU depth increases and the number of MU fibres decreases. Both factors are strongly correlated, as they both affect the amplitude of a MUAP as detected on the skin surface. Shallow MUs with a high number of muscle fibres are expected successfully to resist the influence of noise. For reasons of clarity, we combined the joint influence of all three factors in the following morphological index:

$$I_{f,A} = \frac{1/M \sum_{m=1}^{M} A_m}{f_{fir}} \tag{15}$$

where A_m stands for average peak-to-peak amplitude of a MUAP, as detected by the mth electrode, and f_{fir} denotes the average MU firing rate. The higher the value of the morphological index, the stronger the contribution of the MU to the SEMG recordings. The decomposition results are presented in Table 1. Only the MUs with at least 90% innervation pulses recognised correctly were assumed to be identified.

Identified MUs exhibit almost a perfect match with their reference trains. On average, more than $95 \pm 3.34\%$ of pulses were accurately recognised. The reconstruction of MUAPs also proved to be very robust. In the case of 20 MUs, the average first-norm difference between the original and the decomposed MUAPs, compared with the MUAP amplitude span, yielded 5.1% with an SNR of 20 dB, 6.3% with an SNR of 10 dB and 7.1% with SNR of 0 dB. Owing to space-limitation reasons, the representative results are only briefly exemplified in Figs 1 and 2.

4.2 *Decomposition of real SEMGs*

In the case of real SEMG signals, of course there are no reference innervation trains available. Hence, the performance must be evaluated by other, indirect measures. The ones used in this study were: the regularity of the reconstructed firing patterns, the nature of IPI variability and the shape of the reconstructed MUAPs. Assuming short-term, low-level contractions, the MU innervation trains are known to follow regular, relatively slowly changing pulse patterns.

IPI irregularities are often modelled as realisations of a Gaussian random variable whose maximum value in normal conditions should not exceed the 50% limit of the mean IPI (FARINA and MERLETTI, 2001). Any larger irregularity (in the sense of the discussion above) must therefore be taken as an early warning of a possibly wrong decomposition. Similarly, the reconstructed innervation pulses can be evaluated with respect to the IPI distribution. Several statistical tests (Jarque–Bera, Kolmogorov–Smirnov, Lilliefors etc.) were applied to test the probability that the obtained IPI realisation follow Gaussian distribution (so-called p-value in hypothesis test terminology). A possible non-stationarity of the MU firing rate was compensated by the modelling of the mean IPI as a linear function of time.

The last criterion based on the MUAP shape is the most intuitive one. A single-differential recording technique implies relatively firm limitations to the shapes of MUAPs. Variability is only expected in the peak-to-peak value, the length of MUAPs and minor shape details (mainly in the MUAP tail regions). Furthermore, spatially adjoining electrodes are

Table 2 Number of detected innervation trains, their average firing rate (mean ± SD) and matching of IPI variability with Gaussian distribution calculated by Jarque–Bera statistical test (mean ± SD). Firing patterns were reconstructed from 30 s SEMG signals recorded during isometric 5% and 10% MVC measurements of dominant biceps brachii of five healthy male subjects, as explained in Section 3.2

Contraction level, % MVC	5					10				
Subjects	1	2	3	4	5	1	2	3	4	5
Number of detected MUs	5	4	6	4	6	8	6	7	5	9
Average firing rate, Hz	9.2 ± 0.6	10.3 ± 0.7	11.7 ± 2.1	10.1 ± 0.7	14.5 ± 1.8	14.3 ± 1.3	13.7 ± 1.9	14.2 ± 1.4	13.6 ± 1.6	14.8 ± 2.0
Average probability of Gaussian IPI variability	0.76 ± 0.07	0.70 ± 0.13	0.75 ± 0.11	0.69 ± 0.15	0.72 ± 0.10	0.72 ± 0.08	0.69 ± 0.12	0.73 ± 0.07	0.65 ± 0.17	0.71 ± 0.11

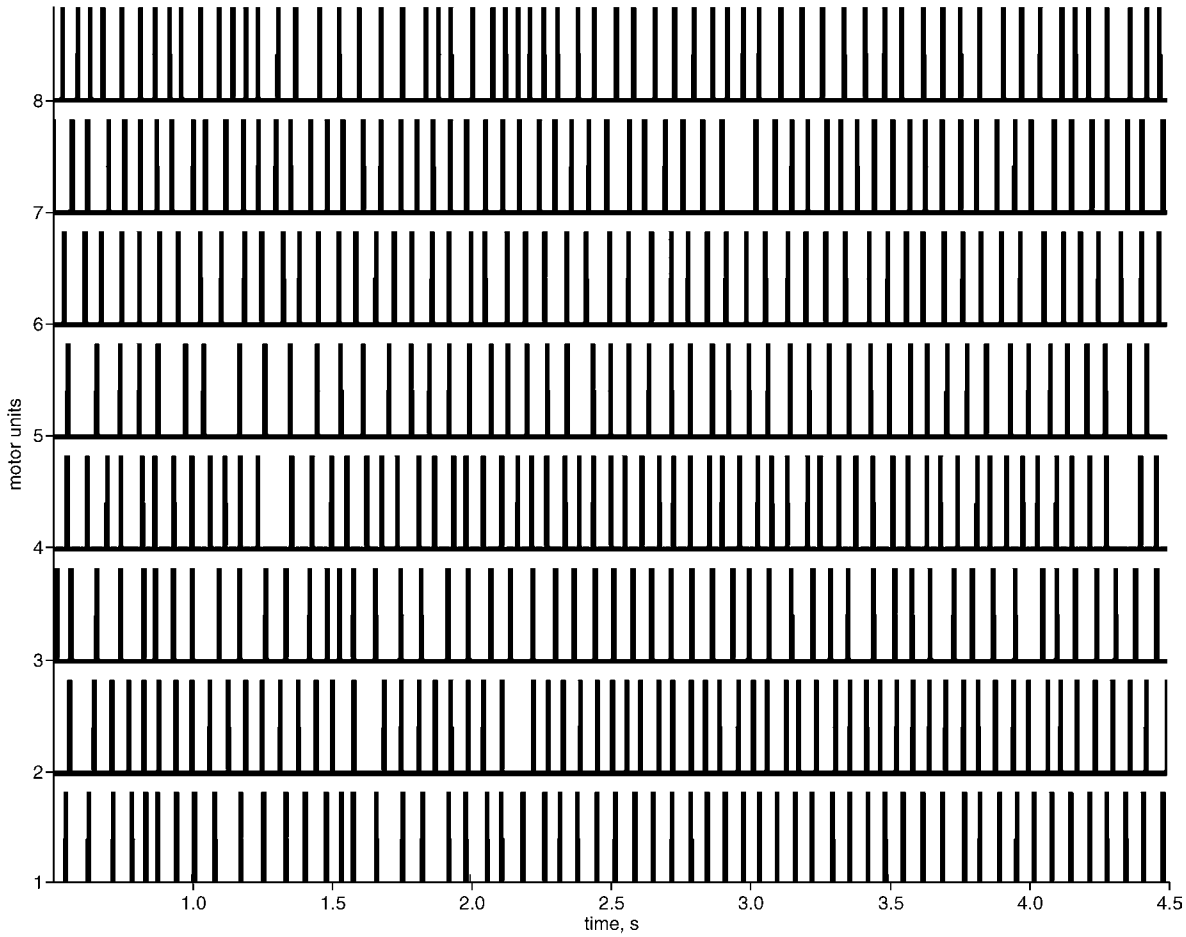

Fig. 3 *MU innervation trains reconstructed from 30 s real SEMG signal. SEMG was recorded during isometric 10% MVC measurement of dominant biceps brachii of subject 1 (age 25 years, height 170 cm, weight 63 kg). Only part of reconstructed innervation trains is depicted*

expected to detect very similar MUAP shapes. By examining the MUAP shape in different channels, the relative positions of the detected MU with respect to the array of electrodes should be traceable. However, above all, the number of successfully reconstructed MU trains was considered the most significant performance criterion. Results are summarised in Table 2. Figs 3–5 depict an example of the decomposition of SEMG signals recorded during the 10% MVC measurement obtained from subject 1.

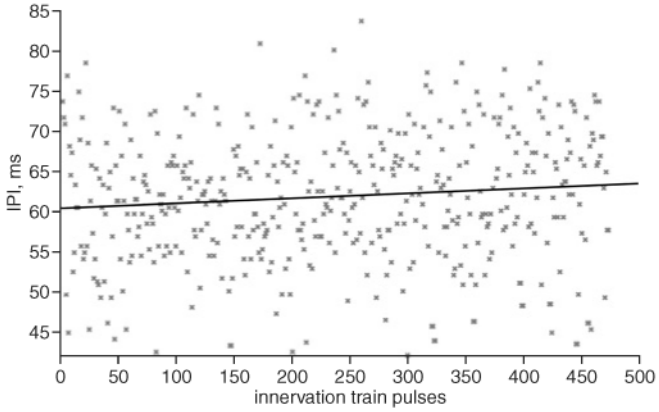

Fig. 4 *(×) IPI variability in innervation pulse train of third MU from Fig. 3. Firing pattern was reconstructed from 30 s real SEMG signal recorded during isometric 10% MVC measurement of dominant biceps brachii of subject 1 (age 25 years, height 170 cm, weight 63 kg). Mean firing rate was estimated 13.6 Hz. (——) Slight decrease of firing rate in time was detected*

5 Discussion

We ran extensive simulations to understand the influence of the most important parameters on a successful SEMG decomposition and, at the same time, to evaluate the performance of our novel decomposition approach. In the cases of five and ten active MUs, almost perfect reconstruction of simulated pulse trains was achieved down to the SNR of 10 dB. The reconstructed MU trains showed a precise match with their reference values. Even more, there was hardly any misplaced pulse (i.e. the so-called true negative statistics). In the case of 20 MUs, only half the active sources were successfully reconstructed. This phenomenon can partly be explained by the fact that there were several MUs active at each arbitrary time moment. A straightforward calculation shows that, having 20 MUs active with an average firing rate of 15 Hz and an average MUAP length of 20 samples, when the measurements are sampled at 1024 Hz, 5.85 sources, $\bar{s}_j(n)$, should be active at each sample position on average.

As stated earlier, the sources with the highest amplitudes are privileged during the reconstruction process, whereas the deeper MUs with lower amplitudes or with strong influence of noise are covered by other stronger MUs. Increasing the sampling frequency brings little benefit as it also increases the average MUAP length (measured in samples). In the case of ten active MUs, the expected average of superimposed MU firings drops to 2.92, and the suppression of weak MUs is not so obvious.

Surprisingly, no significant influence of the MU firing rate was noticed in this study. Although the MUs with low firing rate should theoretically be dominant among successfully reconstructed sources, the results show no significant difference in

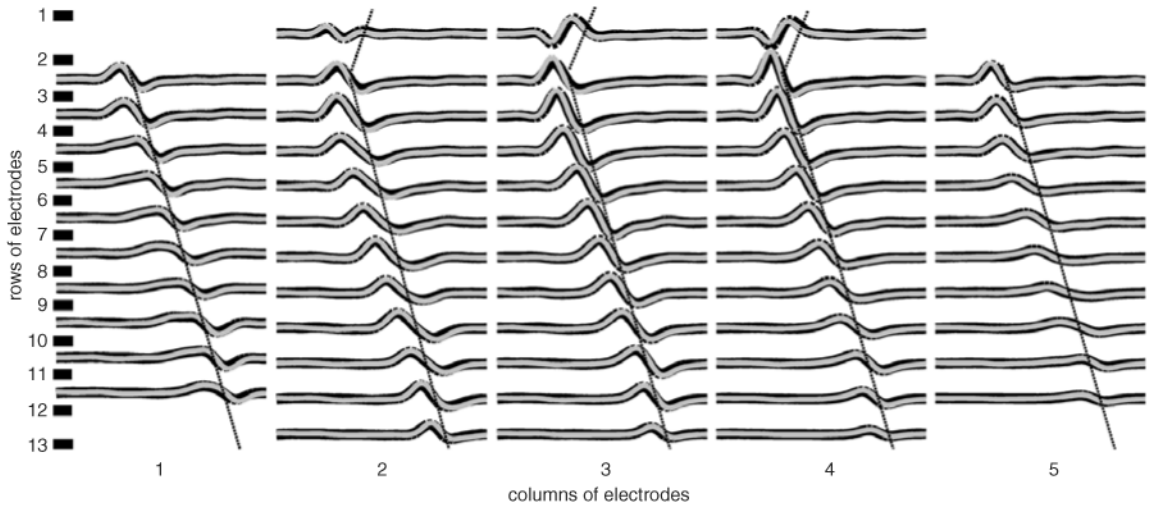

Fig. 5 *MUAPs corresponding to third MU (Figs 3 and 4) reconstructed by spike-triggered sliding window averaging technique from two 10 s intervals (■), one at beginning and (■) other at end of 30 s SEMG signal. Each MUAP is depicted between (■) two adjacent electrodes constituting corresponding single-differential electrode pair (single-differential recording technique was applied to adjacent electrode pairs along columns in electrode array; see Section 3.2). Clear propagation of MUAPs along (– – –) columns of electrode array and, hence, the location of MU innervation zone can be recognised. SEMG was recorded during isometric 10% MVC measurement of dominant biceps brachii of subject 1 (age 25 years, height 170 cm, weight 63 kg)*

the average firing rate between the groups of identified and missed MUs (Table 1). One of the possible explanations could be that a significantly lower noise reduction is achieved through averaging for less active MUs. However, further detailed investigation of this phenomenon is necessary.

As expected, the performance also drops with lower SNRs. At an SNR of 0 dB, only two active MUs were identified on average. The results (Table 1) do not depend on the number of active MUs, which suggests that only the strongest MUs (in the sense of peak-to-peak amplitude) were detected, whereas all the others were treated as background noise. Also, the average value of the morphological index $I_{f,A}$ in Table 1 speaks in favour of this explanation.

The results from the experimental part coincide with those from the simulations. Although no direct evaluation of the proposed decomposition approach was established, much indirect evidence exists. First, all the reconstructed innervation trains exhibit highly regular firing patterns. Secondly, none of the statistical tests applied could reject the hypothesis of Gaussian IPI variability. Finally, the MUAPs reconstructed by the spike-triggered sliding window averaging technique, using the detected MU firings as triggers, show a perfect match with expectations. Not only do they indicate the position of the MU with respect to the electrode array, but they also reveal the innervation zone location and, even the MU conduction velocity.

Our study clearly proves that the proposed decomposition approach successfully resolves the superimpositions of MUAPs, as well as temporal overlapping of the firing patterns. The latter is very important from the physiological point of view, as it enables investigations of short-term MU synchronisation phenomena. The separation of sources, as introduced in Section 2.3, can be considerably affected by noise. Being filtered by the inverse correlation matrix of measurements, the noise appears coloured in the sources, space. The energy of noise in the sources' space therefore depends on the MUAP characteristics.

The greater the differences in MUAPs, the better the conditional number of the correlation matrix of measurements, and, consequently, the smaller the influence of noise. As stated above, different approaches to noise reduction, such as short-term temporal (and spatial) averaging of measurements, repeated reconstruction of sources (13) using different subsets of measurements in each trail, various noise filtering techniques, time-scale processing with wavelets etc., were tested in this study. Their detailed explanation and evaluation reach beyond the scope of this discussion.

6 Conclusions

In this paper, a novel SEMG decomposition approach, suitable for the identification of innervation trains, was introduced and evaluated. A thorough and detailed study of the factors influencing its performance was carried out. As demonstrated by both the simulation and experimental results, the approach is significantly noise-resistant and perfectly resolves not only the superimposition of MUAPs but also the short-term MU synchronisation. The method presented thus contributes a useful tool for the investigation of central motor control strategies, MU recruitment and derecruitment and firing patterns, and for other basic and applied physiological investigations in the field of neurophysiology.

Acknowledgment—The authors are sincerely grateful to Professor Roberto Merletti, Dr Dario Farina and all the members of the LiSiN laboratory at Politecnico di Torino, Italy, for their support in using their SEMG simulator and in the design and implementation of the experimental protocol.

This work was supported by the European Shared Cost Project 'Neuromuscular assessment in the Elderly Worker' (NEW) (contract QLK6-2000-00139) and by the Slovenian Ministry of Education, Science & Sport (contract S2-796-010/21301/2000).

References

AMARI, S. I., HYVARINEN, A., LEE, T. W., and SÁNCHEZ, V. D. A. (2002): 'Blind signal separation and independent component analysis', *Neurocomputing*, **49**, pp. 1–5

BALESTRA, G., FRASSINELLI, S., KNAFLITZ, M., and MOLINARI, F. (2001): 'Time-frequency analysis of surface myoelectric signals during athletic movement', *IEEE Eng. Med. Biol.*, **20**, pp. 106–115

BARROS, A. K., MANSOUR, A., and OHINISI, N. (1999): 'Removing artefacts from ECG signals using independent components analysis', *Neurocomputing*, **22**, pp. 173–186
CLANCY, E. A., and HOGAN, N. (1999): 'Probability density of the surface electromyogram and its relation to amplitude detectors', *IEEE Trans. Biomed. Eng.*, **46**, pp. 730–739
DE LUCA, C. J., FOLEY, P. J., and ERIM, Z. (1996): 'Motor unit control properties in constant-force isometric contractions', *J. Neurophysiol.*, **76**, pp. 1503–1516
DISSELHORST-KLUG, C., RAU, G., SCHMEER, A., and SILNY, J. (1999): 'Non-invasive detection of the single motor unit action potential by averaging the spatial potential distribution triggered on a spatially filtered motor unit action potential', *J. Electromyogr. Kinesiol.*, **9**, pp. 67–72
FALLENTIN, N., JORGENSEN, K., and SIMONSEN, E. B. (1993): 'Motor unit recruitment during prolonged isometric contractions', *Eur. J. Appl. Physiol. Occupat. Physiol.*, **67**, pp. 335–341
FARINA, D., FORTUNATO, E., and MERLETTI, R. (2000): 'Non-invasive estimation of motor unit conduction velocity distribution using linear electrode arrays', *IEEE Trans. Biomed. Eng.*, **47**, pp. 380–388
FARINA, D., COLOMBO, R., MERLETTI, R., and OLSEN, H. B. (2001): 'Evaluation of intra-muscular EMG signal decomposition algorithms', *J. Electromyog. Kinesiol.*, **11**, pp. 175–187
FARINA, D., and MERLETTI, R. (2001): 'A novel approach for precise simulation of the EMG signal detected by surface electrodes', *IEEE Trans. Biomed. Eng.*, **48**, pp. 637–646
GOLUB, G. H., and VAN LOAN, C. F. (1989): 'Matrix computations' (John Hopkins University Press, Baltimore, USA, 1989)
HOLOBAR, A., and ZAZULA, D. (2003): 'Surface EMG decomposition using a novel approach for blind source separation', *Informatica Medica Slovenica*, **8**, pp. 2–14
MERLETTI, R. (1994): 'Surface electromyography: possibilities and limitations', *J. Rehab. Sci.*, **7**, pp. 25–34
MERLETTI, R., KNAFLITZ, M., and DE LUCA, C. J. (1994): 'Myoelectric manifestations of fatigue in voluntary and electrically elicited contractions', *J. Appl. Physiol.*, **77**, pp. 2104–2114
MICERA, S., VANNOZZI, G., SABATINI, A. M., and DARIO, P. (2001): 'Improving detection of muscle activation intervals', *IEEE Eng. Med. Biol.*, **20** (6), pp. 38–47
WEYTJENS, J. L. F., and VAN STEENBERHE, D. (1984): 'The effects of motor unit synchronisation on the power spectrum of the electromyogram', *Biol. Cybern.*, **51**, pp. 71–77
ZAZULA, D., and PLEVIN, E. (2002): 'An approach to decomposition of muscle and nerve signals'. Proc. WSEAS Int. Conf., 2002, Skiathos, Greece, **1**, pp. 1351–1356

Authors' biographies

ALEŠ HOLOBAR received his BS degree in computer science from the University of Maribor, Slovenia, in 2000. He is currently a researcher and a postgraduate student at the Faculty of Electrical Engineering and Computer Science, University of Maribor, Slovenia. His research interests include virtual reality, conceptual learning and signal processing, with current activities focused on blind source separation and biomedical signal processing. He is a member of IEEE, IEEE Computer Society, and Slovenian Society of Pattern Recognition.

DAMJAN ZAZULA received Dipl. Ing., Masters and Doctor of Science degrees in electrical engineering from the University of Ljubljana, Slovenia, in 1974, 1978 and 1990, respectively. After being involved in industrial R&D for 12 years, he joined the Faculty of Electrical Engineering and Computer Science, University of Maribor, Slovenia, in 1987. Currently, he holds the position of Professor in Computer Science, while from 1998 to 2003 he was also appointed as Associate Dean of Research. Dr. Zazula has spent several months as a visiting professor at the ETH in Zurich, Switzerland, and Ecole Centrale de Nantes, France. His main research interests are compound signal decomposition, biomedical imaging, and virtual training tools. He is a member of IEEE, IEEE Signal Processing Society, EURASIP, IAPR, Slovenian Technical Society SATENA, Slovenian Society of Pattern Recognition, and Slovenian Society of Biomedical Engineering.